ACS APPLIED MATERIALS & INTERFACES

www.acsami.org

Research Article

Transformations and Environmental Impacts of Copper Zinc Tin Sulfide Nanoparticles and Thin Films

Sunipa Pramanik, Nancy Trejo, Eileen Mclntire, Natalie V. Hudson-Smith, Beza Tuga, Jiayi He, Eray Aydil, and Christy L. Haynes*

Cite This: *ACS Appl. Mater. Interfaces* 2023, 15, 24978−24988

Read Online

ACCESS | Metrics & More | Article Recommendations | Supporting Information

ABSTRACT: Quaternary chalcogenide copper zinc tin sulfide (CZTS) nanoparticles are used to make the p-type absorber layer in CZTS solar cells, which are considered more benign alternatives to those based on cadmium telluride (CdTe) and less expensive than copper indium gallium selenide. CZTS has an ideal band gap and a high absorption coefficient for solar radiation, making the nanoparticles an attractive option for photovoltaic cells. In this work, we explore the toxicity of CZTS nanoparticles using an environmentally relevant bacterial model *Shewanella oneidensis* MR-1. This study also focuses on understanding the stability of CZTS-based thin films and their direct interaction with bacterial cells. Bacterial cell viability, stability of nanoparticles and thin films, as well as mechanisms of toxicity were evaluated using various analytical tools. The CZTS nanoparticle suspensions show significant acute toxic effects on bacterial cells, but long-term (72 h) exposure of bacterial cells to CZTS-based thin films (made from nanoparticles) do not exhibit similar detrimental impacts on bacterial viability. This result is compelling because it suggests that CZTS nanomaterials will have minimal unintended toxicity as long as they are incorporated into a stable film structure.

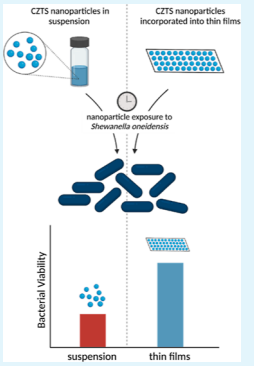

KEYWORDS: *CZTS, solar cells, nanoparticle transformations, nanoparticle thin films, bacterial cell viability*

INTRODUCTION

Because solar energy is a vast resource that can help produce clean, renewable electricity, harnessing solar energy and utilizing it to meet global energy demands has become an extremely important field of research.[1,2] In the last 50 years, due to environmental concerns, solar cells have become one of the leading contenders in renewable energy generation.[3,4] Sustainable solar cell technologies must be based on low-cost, environment-friendly, and Earth-abundant materials in addition to having high-energy conversion efficiencies.[5] Currently, silicon-based solar cells dominate the photovoltaic market owing to their low cost and the abundance of silicon in the Earth's crust.[6,7] However, silicon solar cells cannot be made as thin as CdTe- or CIGS-based solar cells and it is therefore difficult to make flexible. Moreover, they use two orders of magnitude more material than thin-film solar cells, contributing to their manufacturing costs.[8,9] Hence, the search continues for nontoxic thin-film solar cell materials with high absorption coefficients and direct band gaps.[10]

In this search, copper zinc tin sulfide (CZTS) has emerged as one of the potential candidates.[11−15] CZTS has been presumed to have low toxicity because it comprises metals that are less toxic than Cd, such as Cu and Sn. CZTS has a high absorption coefficient (>10^4 cm^{-1} in the visible) and a suitable tunable optical band gap of 1.5 eV.[16] The efficiency of CZTS solar cells has increased over time with optimization of materials and synthetic routes, and the highest reported efficiency to date is 12.6%.[17] The Shockley−Queisser photon balance calculations show that the theoretical limit for CZTS is 32.2%,[18] although various factors are responsible for the lower experimentally obtained efficiency. One of the major reasons for this is the formation of secondary phases and various defects and defect complexes.[7] Research is ongoing to minimize these by using different synthesis techniques and various thin-film deposition approaches to reduce the generation of secondary phases and defects.[19−21] For instance, thin-film deposition processes from hydrazine-based solutions produce high-efficiency solar cells,[22] but hydrazine's toxic and explosive nature renders this route less desirable. Casting CZTS thin films from colloidal nanocrystal dispersions offers a safer method.[15] Nanocrystal-based thin-film coatings, including those composed of CZTS, can be formed through techniques such as drop-casting, dip-coating, spin-coating, and printing.[14]

Even though CZTS nanomaterials and thin films have received significant attention due to their optical properties and use of Earth-abundant, benign metals, studies on these potentially important materials' biological and environmental impacts are insufficient. To the best of our knowledge, one study has been reported investigating the antibacterial

Received: January 9, 2023
Accepted: April 24, 2023
Published: May 10, 2023

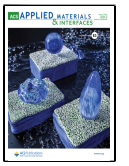

https://doi.org/10.1021/acsami.3c00374
ACS Appl. Mater. Interfaces 2023, 15, 24978−24988

properties of CZTS nanoparticles against pathogenic bacteria, where the goal was to assess the potential application of CZTS nanoparticles as an antibiotic.[23] This study suggests that CZTS nanoparticles have antibacterial effects on Gram-positive and Gram-negative pathogenic bacteria. However, in light of the potential applications of the CZTS nanoparticles, especially in the field of photovoltaics, it is critical to think beyond their application as antibiotics and toward their inevitable unintentional release into the environment.

Bacteria are ubiquitous in the ecosystem, participate in the lowest trophic level in the ecological pyramid, have important roles in decomposition, nutrient cycling, and bioremediation, and thus were chosen as the model organism in this study. Specifically, *Shewanella oneidensis* MR-1 is a robust, Gram-negative, environmentally beneficial bacterial species that has been shown to withstand the negative effects of several engineered nanomaterials, especially when compared to the Gram-positive bacterium, *Bacillus subtilis*.[24,25] Thus, understanding CZTS nanoparticle toxicity mechanisms using *S. oneidensis*can help serve as a benchmark for further comparative studies that could expand to other bacterial species. In our work, CZTS nanocrystal dispersions were synthesized using thermal decomposition of metal diethyldithiocarbamate precursors,[26] and thin films were prepared by drop-casting the nanocrystal suspensions on soda-lime glass.[27] To introduce CZTS nanocrystals to aqueous bacterial suspensions for toxicity assessment, the non-polar moieties on the surface of initially synthesized nanocrystals were exchanged with polar groups, and the CZTS nanocrystals were dispersed in water.[28] Because higher solar cell efficiencies have been observed in CZTS nanocrystal thin films that have been annealed in a sulfur atmosphere at high temperatures,[14,15,29] thin-film stability and bacterial viability studies were performed using both the as-deposited unannealed films as well as annealed thin films. Any potential toxic effects of either the CZTS nanoparticles or thin films on *S. oneidensis* MR-1 were assessed using a drop-plate colony counting assay. Further, mechanisms of nanoparticle toxicity such as metal ion release, damage to the cell membrane via association, and reactive oxygen species (ROS) generation were also explored. Overall, this work demonstrates that, while CZTS nanoparticles in suspension can transform to induce bacterial toxicity, those impacts are largely mitigated when the same nanoparticles are incorporated into an annealed thin film, a promising conclusion for the use of CZTS in photovoltaics.

EXPERIMENTAL METHOD

Materials. Oleic acid (technical grade, 90%), oleylamine (OLA) (technical grade, 70%), and toluene (HPLC grade, 99.9%) were purchased from Sigma-Aldrich. Reagent alcohol (histological grade, 90% ethyl alcohol, 5% methyl alcohol, and 5% butyl alcohol) was purchased from Fisher Scientific. Copper(II), zinc(II), and tin(IV)-diethyldithiocarbamate complexes were synthesized from sodium diethyldithiocarbamate trihydrate (ACS reagent, Sigma-Aldrich) and copper(II) chloride dihydrate (ACS grade, 99+%), zinc chloride (reagent grade, 98%), and tin(IV) chloride pentahydrate (98%), respectively. Sulfur was purchased from Cerac, Inc. (99.999%), and soda-lime glass (SLG) substrates were purchased from Valley Design Corp.

Scanning Electron Microscopy and X-ray Diffraction Characterization. The CZTS nanocrystals were imaged with a JEOL 6500 field-emission scanning electron microscope. The elemental composition was determined using a Thermo-Noran Vantage energy-dispersive X-ray spectrometer installed on the SEM. Raman scattering spectra were collected using a backscattering geometry on a WITec alpha300 spectrometer, an Nd/YAG laser (532 nm), and a DV401 CCD detector. X-ray diffraction (XRD) patterns of the nanoparticles were collected using a Bruker D8 Discover Co Kα radiation source and a 0.8 mm beam collimator. XRD patterns were converted to Cu Kα radiation using JADE analysis software from Materials Data Incorporated.

Synthesis of 5 nm CZTS Nanocrystals. CZTS nanocrystals were synthesized by thermal decomposition of copper diethyldithiocarbamate (107.9 mg), zinc diethyldithiocarbamate (54 mg), and tin diethyldithiocarbamate (106.8 mg) precursors. This procedure was described in Khare et al.[30] The three precursors were dissolved in oleic acid (OA, 4 mL) and 1-octadecene (ODE, 36 mL) and then heated to 60 °C in a 100 mL three-neck flask. The flask was attached to a Schlenk line and degassed and purged with nitrogen three times. After the third nitrogen purge, the flask was heated to 175 °C, and oleylamine (0.9 mL) was quickly injected into the flask. The reaction temperature was maintained at 175 °C for 10 min, after which the flask was cooled naturally to 40 °C. The solution was split equally into two centrifuge tubes. Both centrifuge tubes were centrifuged with reagent alcohol to remove oleylamine (OLA) and unreacted intermediates. After centrifuging for 10 min at 4000 rpm, the supernatant was discarded, and the solid product was dispersed in toluene with 10^{-4} v/v % oleic acid. The dispersions were combined into one vial, and then the solid nanocrystals were precipitated again with centrifugation in reagent alcohol for 10 min. The supernatant was discarded, and the CZTS nanocrystals were dispersed in toluene with 10^{-4} v/v % oleic acid.

Extraction of 5 nm CZTS Nanoparticles in Water. The CZTS nanocrystals, approximately 5 nm in diameter, were extracted into water as described by Tosun et al.[28] First, the nanocrystals were extracted into formamide by mixing 1 mL of CZTS nanocrystal dispersion (~30 mg CZTS per mL toluene with 10^{-4} v/v % oleic acid) with 5 mL formamide and 1 mL of 1.28 g/mL K_2S solution in water. The mixture was stirred for 24 h to extract the CZTS nanocrystals from toluene/oleic acid into the formamide phase. After extraction, the vial containing the CZTS nanocrystals was removed from the stir plate, 2 mL toluene were added, and the mixture was allowed to settle for 5 min. The clear toluene layer at the top was carefully removed with a glass pipet, while the bottom dark formamide layer was transferred into a centrifuge tube with 6 mL acetonitrile. The formamide phase was centrifuged for 10 min at 4000 rpm at room temperature. The supernatant was discarded, and the remaining precipitate was sonicated and dispersed in 4 mL formamide. After the nanocrystals were dispersed, they were precipitated again by centrifuging with 2 mL each of acetone, acetonitrile, and toluene for 10 min. The supernatant was discarded, and the precipitate was dissolved in 4 mL formamide. Precipitation and dispersion in formamide was repeated 1−2 times to remove K_2S. After the last precipitation, the CZTS nanocrystals were dispersed in water.

Synthesis of 40 nm CZTS Nanoparticles and Film Fabrication. CZTS nanocrystals, approximately 40 nm in diameter, were synthesized as described by Chernomordik et al.[26] and used to prepare CZTS films on soda-lime glass substrates. Copper diethyldithiocarbamate (54 mg), zinc diethyldithiocarbamate (30 mg), and tin diethyldithiocarbamate (53.4 mg) precursors were mixed with OA (5 mL) and heated to 60 °C in a 25 mL three-neck flask. In a separate 100 mL three-neck flask, OLA was also heated to 60 °C. Both flasks were attached to a Schlenk line and degassed/purged with nitrogen three times. The flask containing the precursors was heated to 140 °C to dissolve the solids, while the flask containing OLA was heated to 340 °C. The precursor flask was cooled to 75 °C and quickly injected with a syringe into the preheated OLA. After injection, the temperature was maintained for 10 min. The solution was allowed to naturally cool to 40 °C before starting the first centrifugation. OLA and unreacted intermediates were removed by repeated precipitation of the CZTS nanocrystals with reagent alcohol under centrifugation for 10 min at 4000 rpm. The supernatant was discarded, and the solid products were dispersed in toluene with 10^{-4} v/v % oleic acid. The nanocrystals were precipitated a second time

https://doi.org/10.1021/acsami.3c00374
ACS Appl. Mater. Interfaces 2023, 15, 24978−24988

with reagent alcohol, the supernatant was discarded, and the CZTS nanocrystals were finally dispersed in toluene with 10^{-4} v/v % oleic acid. The CZTS nanocrystal dispersions (30 mg/mL) were dropcast onto soda-lime glass substrates to form CZTS films (~1 μm thick). The substrates coated with CZTS film were placed in quartz tubes (10 cm long with 1 cm inner diameter) along with 14 mg sulfur. The quartz tubes were evacuated to 10^{-6} Torr, flame-sealed, and annealed at 600 °C for 1 h.

Bacterial Culture. *S. oneidensis*MR-1 stock was a gift from the lab of Jeff Gralnick at the University of Minnesota. The bacteria were stored at −80 °C before being inoculated onto Luria broth (LB) agar plates and incubated at 30 °C overnight until colonies formed.

Colony-Counting Viability Assays. Colony counting experiments were performed to assess the dose-dependent effect of CZTS nanoparticles at 50, 100, and 200 mg/L concentrations.[25] Currently, there are no data regarding the environmentally relevant concentrations of CZTS nanoparticles, so we used a higher-end concentration to assess the worst-case scenario of accumulation of CZTS particles in the environment and potential bioaccumulation. Bacterial liquid cultures were grown in LB media (Difco LB Broth, Miller) for 4 h at 30 °C to the mid-log phase from colony inoculants on solid agar plates. Bacterial cells were harvested by centrifugation for 10 min at 2000*g* at room temperature, washed in Dulbecco's phosphate-buffered saline (D-PBS) buffer, and suspended in a HEPES buffer (2 mM HEPES and 25 mM NaCl, at pH 7.4). The cultures were then diluted to OD_{600} of 0.2 to achieve a cell density of approximately 2×10^8 cfu/mL. Serial 10-fold dilutions of this bacterial suspension were performed at this stage to achieve a cell concentration of 10^4 cfu/mL in HEPES buffer. The resultant diluted bacterial suspension was treated with 5 nm CZTS nanoparticles at various concentrations (50, 100, and 200 mg/L) and incubated for 15 min. An adapted drop-plate method was used for the *S. oneidensis* cells, where six 10 μL droplets of the exposed bacterial suspensions and untreated negative controls were dropped on an LB-agar plate which had been pre-sterilized under UV illumination for 20 min. The droplets were dried under airflow in a biological cabinet and incubated at 30 °C for 20 h before colonies were counted using a Bantex Colony Counter 920A. The viability of cells from each treatment was reported as a ratio to the negative control samples. The experiments were done using three materials replicates of CZTS nanoparticles repeated three times (three biological replicates) for each batch of nanoparticles.

Ion Dissolution Quantification. Ion dissolution from the CZTS nanoparticles over time in suspension was quantified using inductively coupled plasma mass spectrometry (ICP−MS). The nanoparticles were incubated in HEPES media for 15 min at the same concentrations (50, 100, and 200 mg/L) used for the bacterial viability studies. After the incubation, each suspension was centrifuged using an ultracentrifuge at 61,579*g* for 30 min at 4 °C. The resultant supernatant was collected and used for ICP−MS. The ICP−MS analyses were done on a Thermo Scientific XSeries-2 ICP−MS using CCT/KED mode (Collision Cell Technology/Kinetic Energy Dispersion). The carrier gas was argon, and the CCT gas was a helium/hydrogen blend.

Ion Control Experiments with *S. oneidensis*. The concentration of dissolved metal ions obtained from the ICP−MS data was used to perform ion control experiments with bacteria so that nanoparticle-specific effects could be distinguished from soluble ion effects. *S. oneidensis* were exposed to equivalent concentrations of metal ions for 15 min, and colony-counting experiments were performed. $CuCl_2$, $ZnCl_2$, $SnCl_2$, and $SnCl_4$ were used as the source of ions in these experiments.

Biological Transmission Electron Microscopy Analysis. *S. oneidensis* cultures, with an OD_{600} of 0.8 in HEPES, were exposed to the nanoparticles at 100 mg/L concentration for 15 min, then pelleted, washed thrice with 0.1 M cacodylate buffer solution, and resuspended in a fixation buffer of 2.5% glutaraldehyde in 0.1 M sodium cacodylate buffer and fixed for 50 min. The pellet was washed with sodium cacodylate buffer and dehydrated stepwise with a series of aqueous ethanol solutions of increasing concentrations (30, 50, 70, 80, 90, 95, and 100% ethanol in water). After the washing steps with ethanol, the pellet was washed with propylene oxide three times, and the resin infiltration steps were performed. The pellet was soaked for 2 h in a 2:1 propylene oxide/epoxy resin mixture. This was replaced with a 1:1 propylene oxide/epoxy resin mixture, and the pellet was incubated in this mixture overnight. After this, the pellet was incubated in a fresh batch of 1:1 propylene oxide/epoxy resin mixture for 6 h and finally placed in a pure resin mixture and infiltrated overnight. The resin sample was then cured in an oven at 40 °C for one day and then at 60 °C for two days. Ultrathin sections (65 nm-thick) were sectioned using a Leica UC6 microtome and a Diatome diamond knife and stained with uranyl acetate and lead citrate. These sections were placed on copper TEM grids (Ted Pella Inc.), and imaging was done using an FEI Tencai T12 TEM while negative control *S. oneidensis* images were prepared using the same methods but imaged using the Tecnai G2 Spirit BioTWIN transmission electron microscope.

Total ROS Generation Analysis. An abiotic assessment of ROS generation in HEPES buffer media (in the absence of bacteria) was performed using the 2′,7′-dichlorofluorescein diacetate (DCFDA, also known as H_2DCFDA) assay.[31,32] DCFDA in DMSO stock solution (20 mM) was diluted 100-fold in HEPES buffer. Then, 50 μL of DCFDA working solution was mixed with 200 μL of CZTS nanoparticle solution at 50, 100, or 200 mg/L. A negative control for the experiment was performed by adding the DCFDA solution to the HEPES buffer, while a positive control experiment was done by adding the DCFDA solution to 1 M hydrogen peroxide solution. Each condition in the experiment was performed in triplicate in a 96-well optical bottom plate (Costa, Corning, NY). The fluorescence counts were recorded by a Synergy 2 Multi-Mode microplate reader (BioTek, Winooski, VT) at Ex/Em: 485/525 nm for 2.5 h.

Bacterial Exposure to CZTS Thin Films. *Short-Term (15 min) Incubation of Thin Films with Bacteria.* *S. oneidensis* were grown for 4 h in LB broth and then washed with DPBS and diluted in HEPES buffer to an OD_{600} of 0.2 (2×10^8 cfu/mL). 1 mL of bacterial solution was dropped on top of the thin film (either annealed or unannealed), left to sit for 15 min, then pipetted out, and diluted to a cell concentration of 10^4 cfu/mL via serial dilution. The exposures were done simultaneously in triplicate with annealed and unannealed thin films. The controls for the experiment included cells incubating on a soda-lime glass substrate without CZTS nanoparticles and cells not exposed to anything. After the serial dilution, 10 μL aliquots of the bacterial suspensions were dropped on an LB-agar plate, including the negative controls, and the plates were incubated at 30 °C for 20 h. The number of colonies on the plate corresponding to each exposure condition was counted the next day using a Bantex colony counter 920A.

Long-Term (72 h) Incubation of Thin Films with Bacteria. Since the bacterial cells do not remain viable in HEPES buffer for extended periods, the cells were subject to prolonged exposure in LB broth media and aqueous minimal media (buffered with 10 mM HEPES and containing 11.6 mM NaCl, 4.0 mM KCl, 1.4 mM $MgCl_2 \cdot 6H_2O$, 2.8 mM Na_2SO_4, 2.8 mM NH_4Cl, 0.088 mM Na_2HPO_4, 0.051 mM $CaCl_2$, and 100 mM sodium lactate as a nutrient source). *S. oneidensis* was grown in LB broth overnight, then washed with DPBS, and suspended in either LB broth or minimal media (depending on the final exposure media). The OD was adjusted to 0.2, and 1 mL aliquots of the diluted cell suspensions were pipetted into 9 mL of fresh media. The CZTS thin films were introduced into the culture tubes and incubated in a rotary shaker at 30 °C for 72 h. The exposures were done simultaneously with 3 annealed and 3 unannealed thin films. The controls for the experiment included cells incubating on a soda-lime glass substrate without added CZTS and cells not exposed to anything. After the 72 h period, aliquots of the exposed bacterial suspensions were collected, diluted to cell concentrations of 10^4 cfu/mL, and the drop-plate colony counting assay was performed. Additionally, culture tubes with the media (without any bacteria) and the films were incubated simultaneously under the same conditions, aliquots were collected, and ICP−MS was performed to assess any dissolution to constituent ions.

https://doi.org/10.1021/acsami.3c00374
ACS Appl. Mater. Interfaces 2023, 15, 24978−24988

Thin-Film Incubation with MQ Water, HEPES, or Artificial Seawater. CZTS thin films were incubated in three different media for 72 h; then, aliquots of the exposed media were collected, and ICP−MS was performed to characterize thin-film transformation.

RESULTS AND DISCUSSION

Synthesis and Characterization of CZTS Nanoparticles and Thin Films. The synthesized nanoparticles were imaged with a scanning electron microscope as shown in Figure 1; high-resolution transmission electron microscopy

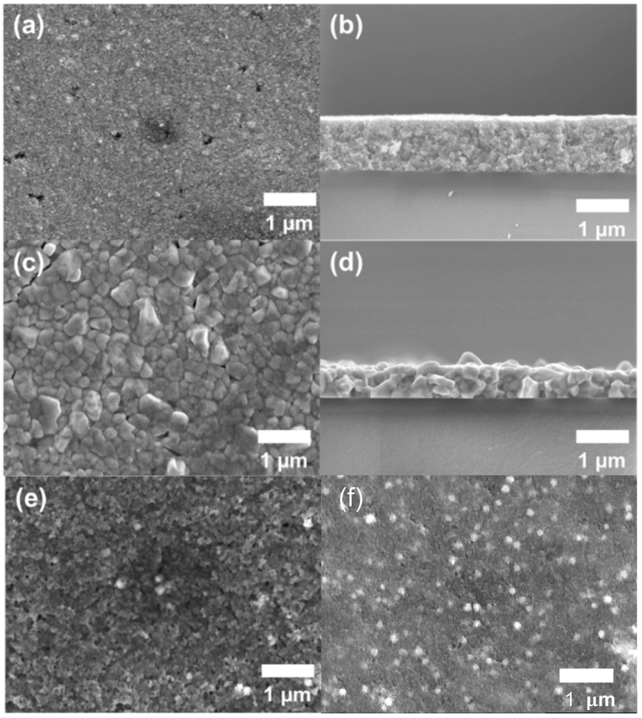

Figure 1. Scanning electron micrograph top view and cross-sections CZTS NP films made from 40 nm diameter of CZTS crystals (a,b) before annealing and (c,d) after annealing at 600 °C for 1 h in a sulfur atmosphere. Scanning electron micrograph for (e) 5 nm diameter CZTS NPs and (f) 40 nm diameter CZTS NPs not incorporated into thin films.

(TEM) images and XRD data for these nanoparticles were published in previous work.[30] The CZTS NP films were ∼1 μm thick before annealing and ∼0.6 μm thick after annealing. The film grains grew to 250 ± 100 nm after annealing. Energy-dispersive X-ray spectroscopy (EDS) revealed near-stoichiometric ratios of Cu, Zn, Sn, and S. Specifically, it can be observed from EDS that the 5 nm diameter CZTS NPs (Figure S1a) were composed of 20.4% Cu, 17.8% Zn, 12.9% Sn, and 48.8% S, while the 40 nm diameter CZTS NPs (Figure S1b) contained 29.2% Cu, 15.2% Zn, 12.2% Sn, and 43.5% S. After annealing, the films composed of 40 nm diameter CZTS NPs (Figure S1c) displayed an elemental composition of 29.4% Cu, 13.9% Zn, 11.2% Sn, and 45.5% S; this composition change was expected based on the sulfur atmosphere used during annealing.

XRD from the NPs revealed the presence of the expected CZTS phase as shown in Figure 2. All XRD diffraction peaks match with diffraction from the CZTS kesterite phase (ICDD ref 00-026-0575). The diffraction peak widths decrease with increasing NP size and with annealing treatment. Larger NPs

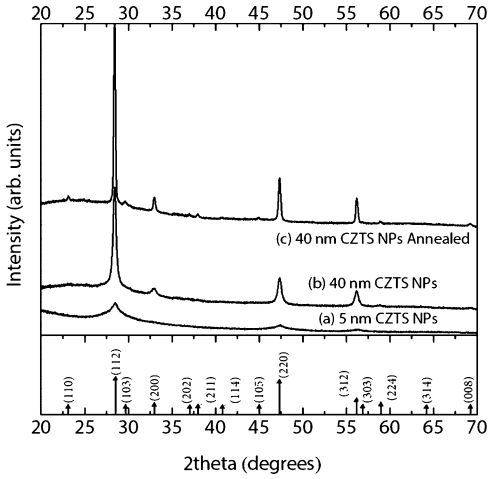

Figure 2. XRD of (a) 5 nm diameter CZTS NPs, (b) film with 40 nm diameter CZTS NPs, and (c) film with 40 nm diameter CZTS NPs after annealing at 600 °C for 1 h in a sulfur atmosphere.

and annealed NPs have larger crystals with more planes available to strengthen the diffraction signal. The number of matching diffraction peaks to CZTS increases with NP size and with annealing treatment. Both the 5 nm diameter NPs and films made from 40 nm diameter NPs show diffraction from the (112), (220), and (312) planes, but the films with 40 nm diameter NPs also show diffraction from the (200) and (224) planes. Annealing the films with 40 nm diameter NPs results in additional diffraction from the (110), (103), (202), (211), (224), and (008) planes. The CZTS diffraction pattern shares similar peaks with ZnS and tetragonal Cu_2SnS_3.[33] However, the diffraction peaks from (202) and (211) are absent in ZnS and are small in tetragonal Cu_2SnS_3. Therefore, the presence of the CZTS phase is confirmed in the annealed films made with 40 nm diameter NPs.

Raman spectroscopy was performed to confirm the phases of the 5 nm diameter NPs and the films cast from 40 nm diameter NPs. XRD combined with Raman spectroscopy can unambiguously confirm the CZTS phase. Figure S2 shows the Raman spectra for 5 nm diameter NPs, films with 40 nm diameter NPs, and films made from 40 nm diameter NPs after annealing. All three spectra reveal the characteristic peak for CZTS at ∼336−338 cm^{-1} shift. This peak can be assigned to the A mode of kesterite CZTS.[34] The 5 nm diameter CZTS NPs exhibit a weak, broad peak due to phonon confinement in smaller nanoparticles. Taken together, the CZTS phase was confirmed within the detection limits of EDS, Raman spectroscopy, and XRD.

Bacterial Viability Assays and Investigation of Mechanisms of Toxicity. *Colony-Counting Bacterial Viability Assays.* Drop-plate colony counting assays were performed to assess bacterial cell viability after exposure to CZTS nanoparticles. The concentration of bacterial cells at which distinct and non-overlapping colonies can form was first ascertained, and the diluted bacterial suspensions were exposed to CZTS nanoparticle solutions at increasing concentrations of 50, 100, and 200 mg/L. Since the number of colonies that form on the LB-agar plate after a 20 h incubation indicates the number of viable cells present in the suspension during nanoparticle exposure, any decrease in the number of colonies compared to the negative controls indicates toxic effects of nanoparticles or nanoparticle transformation products.

https://doi.org/10.1021/acsami.3c00374
ACS Appl. Mater. Interfaces 2023, 15, 24978−24988

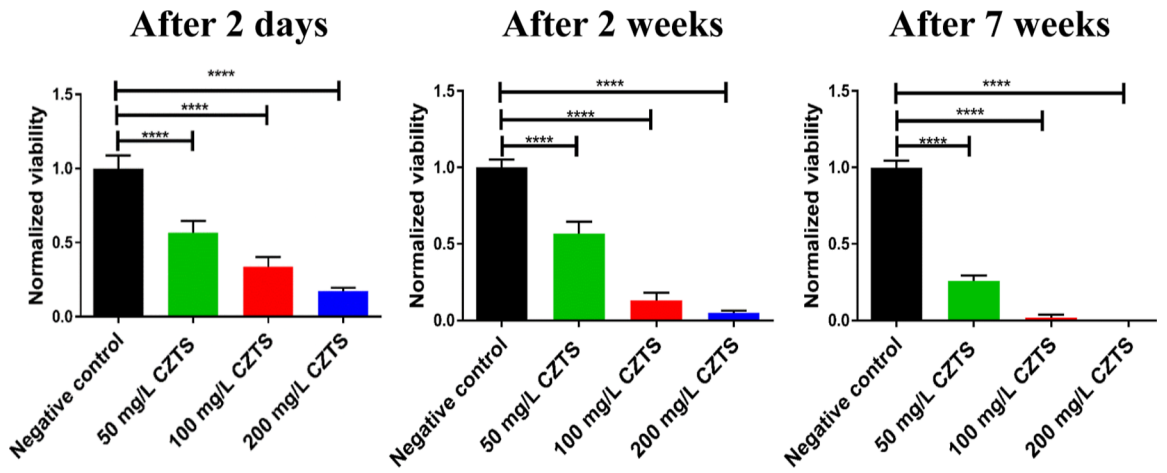

Figure 3. Bacterial viability of *S. oneidensis* in the presence of 5 nm diameter CZTS nanoparticles after various post-synthesis aging times (as noted) as indicated by drop-plate colony counting. Statistical analysis for these experiments was performed using one-way ANOVA, followed by post-hoc Tukey's multiple comparisons tests (GraphPad Prism software, La Jolla, CA). All values plotted are the mean ± standard deviation (SD), and the statistical significance is indicated using asterisks (p values < 0.0001 indicated by ****, 0.0001 to 0.001 indicated by ***, 0.001 to 0.01 indicated by **, and 0.01 to 0.05 indicated by *).

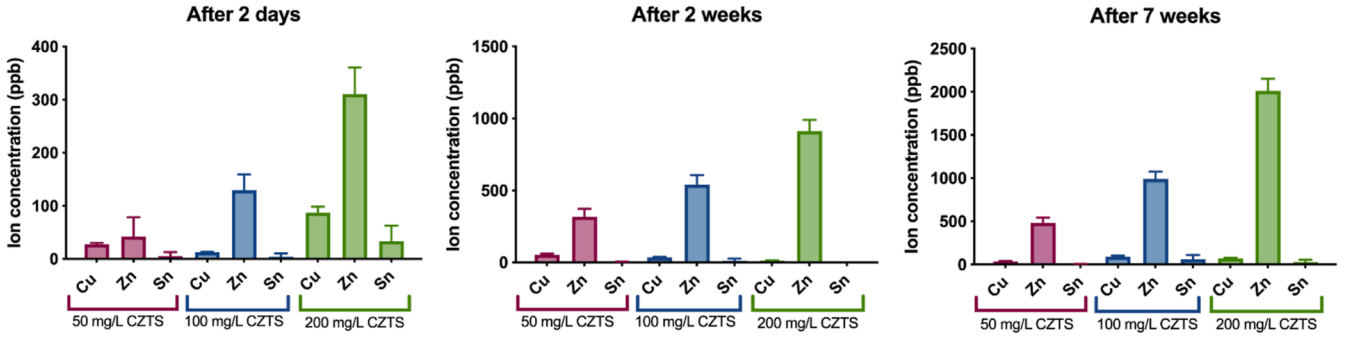

Figure 4. Dissolved metal concentrations as obtained by ICP−MS from 5 nm-diameter CZTS nanoparticle suspension 2 days, 2 weeks, and 7 weeks after initial nanoparticle synthesis. Note the different y-axis scale between the three different timepoints.

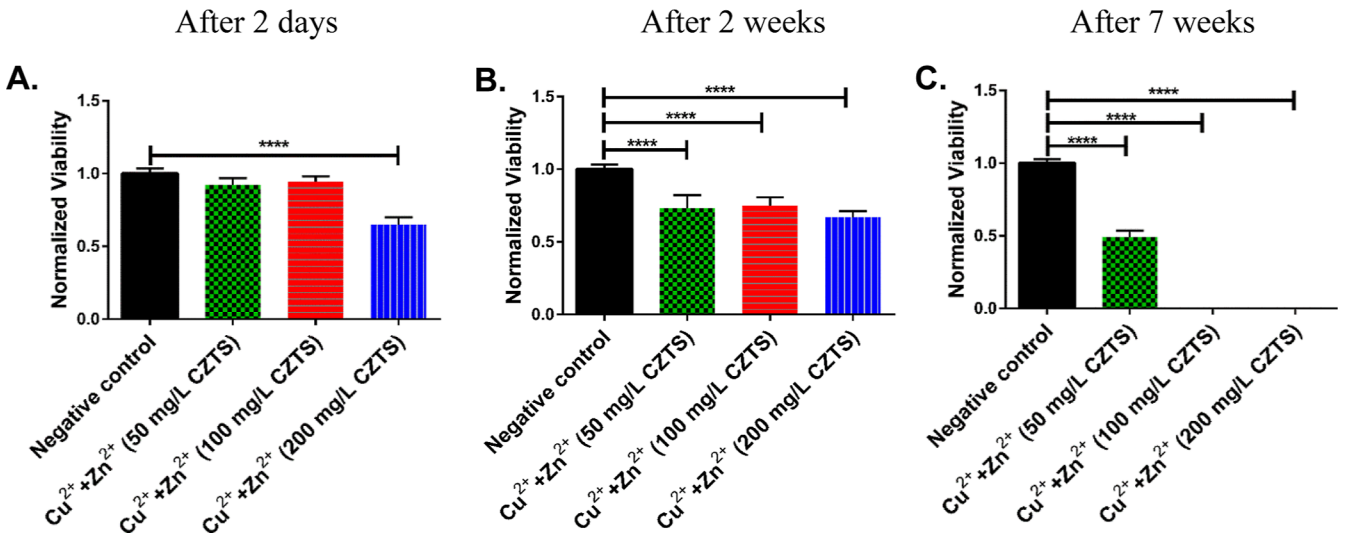

Figure 5. Bacterial viability results after being exposed to Cu^{2+} and Zn^{2+} ion concentrations corresponding to those measured from 50, 100, and 200 mg/L CZTS nanoparticle suspensions at (A) 2 days, (B) 2 weeks, or (C) 7 weeks after nanoparticle synthesis. The ion exposure experiments were repeated twice (two biological replicates) with three analytical replicates for each condition. Statistical analysis for these experiments was performed using one-way ANOVA, followed by post-hoc Tukey's multiple comparisons tests (GraphPad Prism software, La Jolla, CA). All values plotted are the mean ± SD, and the statistical significance is indicated using asterisks (p values < 0.0001 indicated by ****, 0.0001 to 0.001 indicated by ***, 0.001 to 0.01 indicated by **, and 0.01 to 0.05 indicated by *).

https://doi.org/10.1021/acsami.3c00374
ACS Appl. Mater. Interfaces 2023, 15, 24978−24988

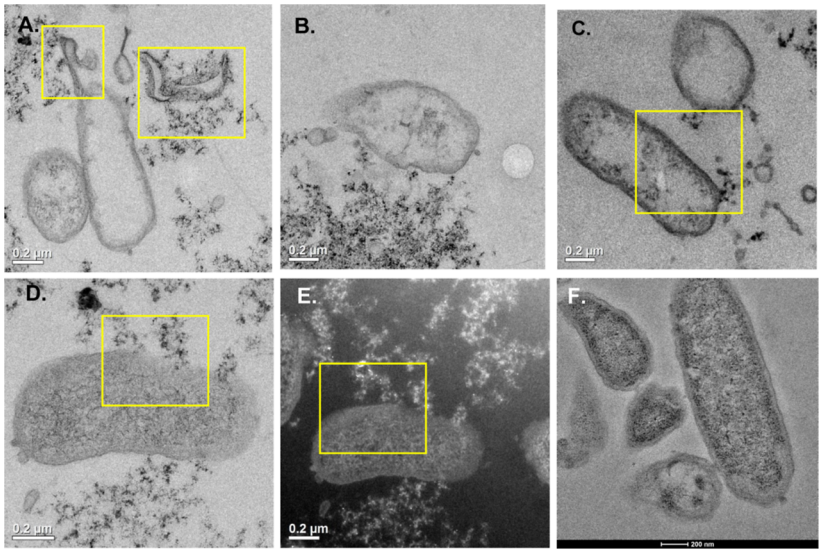

Figure 6. Biological TEM images of *S. oneidensis* after being exposed to 5 nm diameter CZTS nanoparticles in suspension exhibiting (A) severe cellular membrane damage and (B) association of nanoparticles with the bacterial cell membrane. Images (C,D) show more cell membrane association of nanoparticles and (E) is the dark-field counterpart of (D). (F) shows negative control *S. oneidensis* images with no nanoparticle treatment.

In this experiment with the aqueous CZTS (5 nm diameter) nanoparticle suspension, significant toxic effects on bacterial colony formation were observed. In addition, an increase in the toxic effect was observed over time, depending on how long the nanoparticle suspension was used after synthesis, indicating that the CZTS nanoparticles transform as they age. Bacterial exposure experiments were performed 2 days, 2 weeks, and 7 weeks after the initial synthesis of nanoparticles to characterize this effect, and the results are shown in Figure 3. Each experiment was repeated with 2 batches of materials (2 material replicates) and was performed two times to obtain two biological replicates, while each biological replicate included three technical replicates.

It is clear from the data in Figure 3 that the 5 nm diameter CZTS nanoparticles become more toxic to bacteria as they age. The observed toxicity could be due to several factors such as dissolved ions, disruption of cell surface structures, DNA damage, or ROS generation based on NP transformation. The observation of increasing toxicity over time due to gradual ion dissolution has been reported in other nanomaterial studies such as those with lithiated nickel manganese cobalt oxide and Ag NPs[35−37] and thus was considered a likely culprit here. While we cannot directly calculate the concentration at which 50% of bacteria are killed in this experiment (or LC_{50} value), Figure 3 suggests that it likely lies between 50 and 100 mg/L of CZTS.

Ion Dissolution Quantification. To assess the concentration of dissolved ions in the solution, the 5 nm diameter CZTS nanoparticle suspensions were incubated in HEPES buffer and then ultracentrifuged to separate the nanoparticles. The supernatants were collected, and the presence of dissolved metal was quantified using ICP−MS as shown in Figure 4. An increasing trend in the dissolution of Zn was observed with increasing concentration of CZTS suspension and increased time gap after synthesis.

Ion Control Experiments. Bacterial viability was monitored in the presence of metal ions, using ion concentrations as obtained from ICP−MS in the previous section. On exposure to only Zn^{2+} ions, no significant decrease in bacterial cell viability was observed, except in the case of the highest concentration of Zn^{2+} ions at 2012 ppb, where the viability was still at 81%. After the addition of Cu^{2+} ions with the Zn^{2+} ions, drastic decreases in cell viability were observed (Figure 5). Synergistic toxicity of heavy metals such as copper and zinc is a possibility and has been reported previously.[38] The effects of heavy metals such as copper and zinc on microorganism growth are widely studied in the literature.[39] Heavy metals can inhibit cellular function through oxidizing vital enzymes, replacing critical metals in biomolecules, or interacting with DNA. Even though copper is an essential micronutrient for living organisms, it is also known for its antimicrobial properties. Cu^{2+} ions can bind with the sulfhydryl groups in proteins and enzymes and thus hinder normal cellular metabolism.[40] Zn^{2+} ions can prohibit the function of the Mg^{2+} transporter MgtA by competing as substrates.[41] These effects may contribute to the toxic effects of the CZTS nanoparticle dispersion due to the production of dissolved ions. However, a comparison between Figures 3 and 5 reveals that the decrease in viable bacterial colonies measured following exposure to the CZTS nanoparticle suspension is still not completely explained by the presence of increased Cu^{2+} and Zn^{2+} ions.

One thing to keep in mind is that the slow release of ions from the nanoparticles might have a different impact on the bacterial viability than a single dose of ions used in the case of ion control experiments. In addition, nanoparticles may interact with the bacterial surface, generating large localized ion concentrations as the CZTS transforms.

Only small amounts of tin were detected in the supernatant, and we were interested in assessing the effect of tin ions on bacteria. However, most tin compounds are polar covalent compounds, so ion control experiments with tin compounds are difficult. We attempted to use $SnCl_2$ and $SnCl_4$ as our tin ion controls, but any observed effects could be due to the compound rather than the tin ions. Upon introducing $SnCl_2$ and $SnCl_4$ to the bacterial suspension (Figure S3), an increase in toxicity was observed compared to the Cu^{2+} + Zn^{2+} controls. The toxic effect of the combined ions after adding the tin

https://doi.org/10.1021/acsami.3c00374
ACS Appl. Mater. Interfaces 2023, 15, 24978−24988

compounds was even more than that observed with just the nanoparticle dispersion. This result suggests that the toxic effect observed after adding the tin compounds is indeed due to the tin compounds rather than the tin ions from the CZTS nanoparticles.

Biological TEM Analysis. Biological TEM helps with the qualitative assessment of nanoparticle interaction with bacterial cells and provides an excellent tool to visualize any association of nanoparticles with cells. Figure 6 shows the results obtained after treating the *S. oneidensis* cells with 100 mg/L of 5 nm diameter CZTS nanoparticle suspensions as well as negative control bacterial cells.

As seen in the images in Figure 6, the 5 nm diameter CZTS nanoparticles inflict severe damage on *S. oneidensis* cells; as smaller-diameter nanoparticles have a higher surface-area-to-volume ratio (and the surface tends to be the more reactive nanoparticle component), interrogating the 5 nm diameter reveals the "worst-case scenario" among the nanoparticles and films considered herein. In image A (Figure 6), the nanoparticle clusters are against the cell membrane, and a disintegrated cell membrane structure surrounded by nanoparticles is observed. Other images show nanoparticle association with the cell membrane, and as seen in image C, partial disruption of the cell membrane. Image E is a dark-field version of the bright field image D. Dark-field TEM imaging can help identify crystalline nanoparticles in a biological matrix due to electron scattering from nanoparticles with high mass and crystallinity as opposed to the matrix around them, which makes them appear bright against a dark background.[42] Based on previous research, we hypothesize that lipopolysaccharides (an outer cell wall component of Gram-negative bacteria) is a critical player in the CZTS NP/bacterial membrane interaction. Future work will explore this molecular-level interaction using bacterial mutants or various bacterial strains. It is evident from the images that the association of the nanoparticles with the bacterial cells likely contributes to severe damage of the cell structures, affecting cell viability and colony formation. These are representative images obtained after investigating at least 20 bacterial cells on two TEM grids.

ROS Generation Assay. Semiconductor nanoparticles such as CIGS and CdSe have been reported to produce ROS from photogenerated electron/hole (e^-/h^+) pairs and subsequent reactions.[43−45] Such reactions are especially likely in CZTS in the presence of ambient light because its 1.5 eV band gap allows for significant absorption. While ROS occur naturally and are managed in biological systems, excess ROS can be harmful as they may induce macromolecule oxidation, changes in gene transcription, as well as damage to cell organelles.[46]

The DCFDA assay was performed to assess the ROS generation from 5 nm diameter CZTS nanoparticles. As observed from Figure 7A, nanoparticle dose-dependent ROS generation was observed. To obtain a clear view of the CZTS nanoparticle ROS generation, the data were plotted without the very large positive control response to 1 M H_2O_2 (Figure 7B). From this plot, it is evident that there is a progressive increase in the ROS generation over the incubation time. Based on these data, it can be inferred that CZTS nanoparticles produce or induce ROS, and the amount of ROS generated is directly related to the nanoparticle concentrations and incubation times. These studies focused on obtaining preliminary information about the ROS generation by CZTS nanoparticles; however, future work will incorporate other fluorescent dyes to further assess ROS

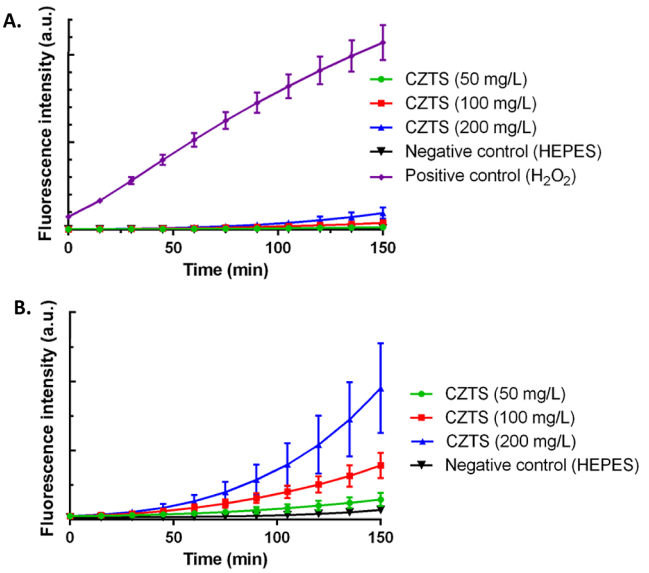

Figure 7. (A) Abiotic ROS generation by 5 nm diameter CZTS nanoparticles assessed using the DCFDA assay. (B) Data as shown in (A), but without the positive control to more easily visualize the CZTS-specific ROS generation.

production, facilitate quantification, and clarify the specific, relevant ROS species.

Bacterial Incubation with CZTS Thin Films. Toxicity studies are generally done using nanoparticle dispersions, and it is not common to assess the toxicity of nanoparticle-based thin films. However, as the absorber material in solar cells, CZTS nanoparticles will be potentially used in commercial products as thin films. Thus, at the time of their disposal, they may enter the environment as thin films. It is therefore of interest to assess how these thin films will behave in different media and affect bacterial viability. A larger primary nanoparticle size of 40 nm was used for these thin film studies based on optimized processing conditions for making thin films.

Short-Term Exposure to 40 nm Diameter CZTS Nanoparticle Thin Films. After short-term exposure of *S. oneidensis* bacterial suspension on CZTS (40 nm diameter) thin films for 15 min, the bacterial cells were collected, diluted, and 10 μL aliquots were dropped onto LB-agar plates. The experiment was done with three annealed and three unannealed films, along with three glass substrates as negative control surfaces. After overnight incubation, no statistically significant changes in bacterial viability (number of colonies formed) were observed compared to the negative controls (Figure 8).

Longer-Term Exposure to 40 nm Diameter CZTS Nanoparticle Thin Films. For a longer-term comparison, both annealed and unannealed thin films were incubated in the presence of bacterial cells in nutrient-rich LB medium as well as relatively nutrient-sparse minimal media with lactate. The exposures were carried out for 72 h. Following exposure, 10 μL droplets of the exposed bacterial suspensions were placed on LB-agar plates to perform standard colony counting assays. In addition, ICP−MS was performed on media exposed to thin films under the same conditions without the bacteria to characterize any dissolution from the thin films.

For both the LB-broth media and minimal media, no significant differences in colony counts were observed compared to the negative controls even after 72 h of exposure. In LB-broth, ion dissolution was quantified using ICP−MS as

https://doi.org/10.1021/acsami.3c00374
ACS Appl. Mater. Interfaces 2023, 15, 24978−24988

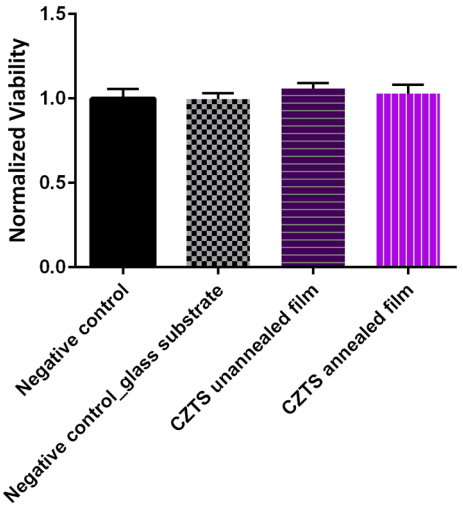

Figure 8. No significant toxic effect was observed upon incubating the bacterial suspension over nanoparticle-assembled CZTS thin films for 15 min.

shown in Figure 9A. It is notable that annealing significantly impacts the dissolution profile of the CZTS thin films. Thus, we hypothesize that even if the dissolved ions had a detrimental effect on some portion of the first generation of cells, the surviving bacteria were able to recover in subsequent generations after long exposure, especially in the presence of nutrient-dense LB broth. Surprisingly, no significant toxic effect was observed in a nutrient-sparse minimal media either (Figure 9D). Figure 9C shows the ion dissolution data of the thin films in minimal media. From the ion dissolution data, it can be concluded that the unannealed films leach more copper and zinc ions, whereas the annealed films leach more tin.

Thus, even though significant negative impacts on colony formation were observed for *S. oneidensis* upon exposure to CZTS nanoparticles in suspension, no toxicity was observed upon exposure to CZTS nanoparticle thin films within the time frame of the experiments performed herein. Initially, we thought that the non-toxic effect of the CZTS thin films was at least in part due to the much lower specific surface area of the thin films composed of 40 nm diameter nanoparticles, leading to less ion dissolution from the annealed thin films compared

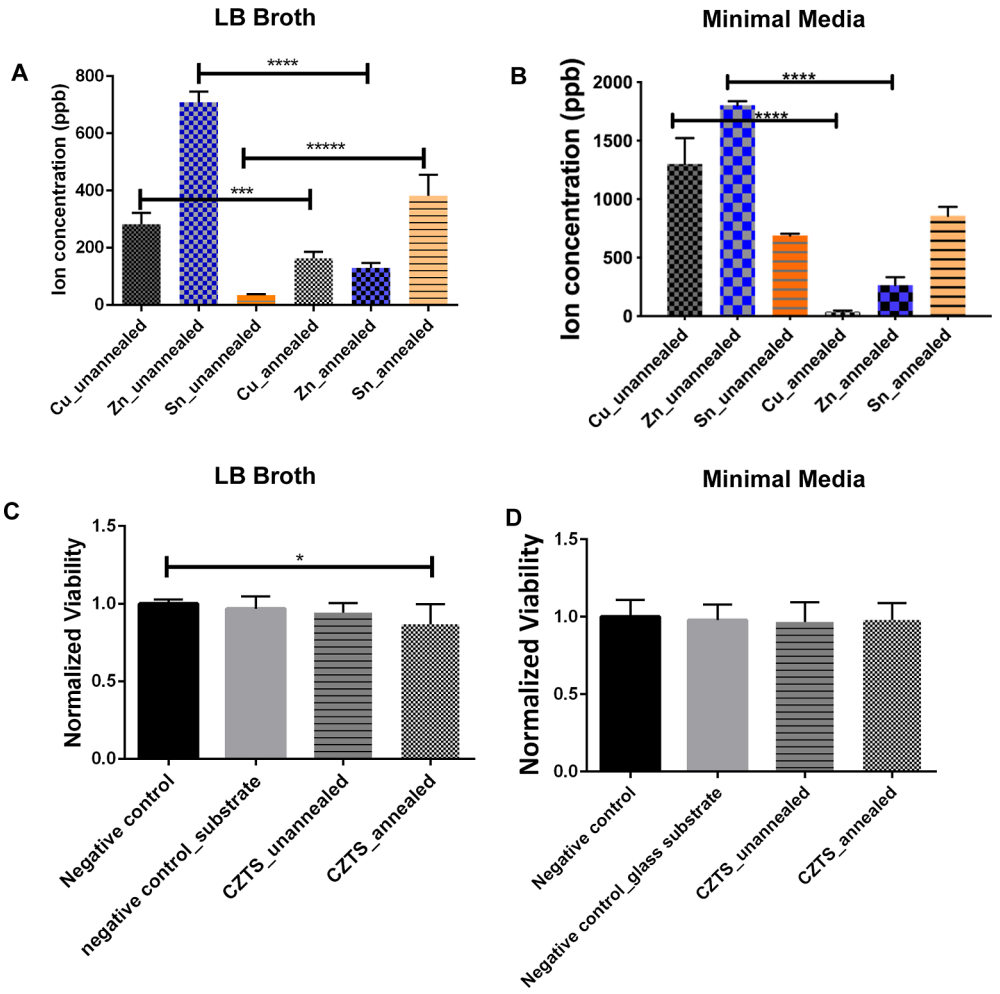

Figure 9. Ion dissolution from the unannealed and annealed CZTS films in (A) LB broth and (B) minimal media. For (C) LB broth exposure, no significant loss in bacterial viability, as measured by colony formation, is observed in the case of unannealed films and only slight loss in viability is observed in the case of the annealed films. For minimal media exposures (D), no significant loss in viability is observed in the case of unannealed or annealed films. Statistical analysis was performed using one-way ANOVA, followed by post-hoc Tukey's multiple comparisons tests (GraphPad Prism software, La Jolla, CA). All values plotted are the mean ± SD, and the statistical significance is indicated using asterisks (p values < 0.0001 indicated by ****, 0.0001 to 0.001 indicated by ***, 0.001 to 0.01 indicated by **, and 0.01 to 0.05 indicated by *).

https://doi.org/10.1021/acsami.3c00374
ACS Appl. Mater. Interfaces 2023, 15, 24978−24988

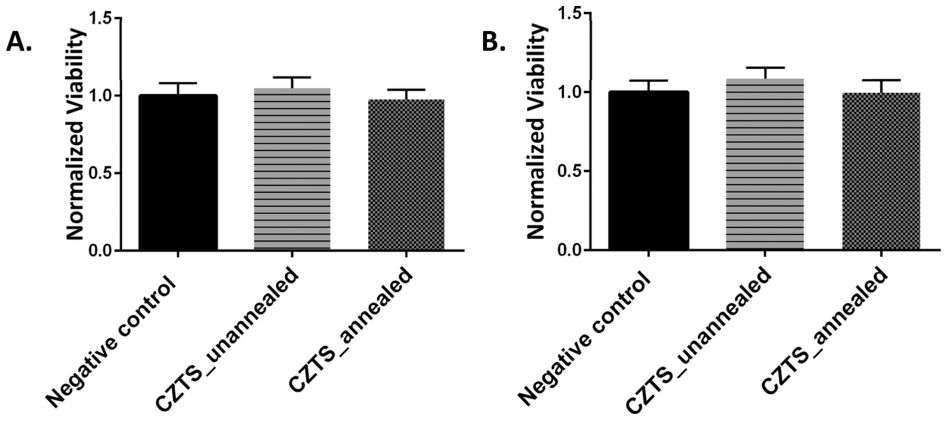

Figure 10. No significant loss in viability is observed for unannealed or annealed films made using 5 nm diameter CZTS nanoparticles in (A) LB media or (B) minimal media over an exposure period of 72 h.

to the 5 nm diameter nanoparticles in solution. Simple estimates assuming unchanged density for the 5 nm diameter and 40 nm diameter CZTS nanoparticles and that half of the 40 nm diameter specific surface area is lost during incorporation into the thin film suggests a 16 times lower specific surface area in the thin film system than for suspended 5 nm diameter CZTS nanoparticles. However, the ion dissolution data show that neither unannealed nor annealed films show 16 times lower ion release. For annealed films, less Cu^{2+} is released, but more Sn ions are released. For unannealed films, all dissolved ion concentrations are higher than those from the 5 nm diameter nanoparticles in solution. Clearly, the change in toxicity cannot simply be a function of the differences in specific surface area of the presented nanostructures. Overall, this is a positive development in using CZTS thin films, especially since no toxic effect was observed even in minimal media, mimicking the nutrient-scarce natural environment. It will be interesting to see future work involving other more complex organisms and gene expression and chronic exposure studies.

Long-Term Exposure with 5 nm Diameter CZTS Nanoparticle Thin Films. 5 nm diameter CZTS particles are generally not considered suitable candidates for thin-film preparation due to their tendency to produce voids and cracks in the thin films, leading to shorts.[36] Nevertheless, similar experiments were completed with thin films made from 5 nm diameter CZTS nanoparticles to explore any difference in toxicity of these particles in thin films compared to the 40 nm diameter nanoparticle thin films (based on suspension-phase negative impacts).

As with the 40 nm diameter CZTS nanoparticle thin films, no significant loss in bacterial viability was observed in either LB or minimal media (Figure 10). Thus, it can be concluded that thin films made out of 5 nm diameter nanoparticles, as well as 40 nm diameter nanoparticles, do not pose any viability threats to *S. oneidensis* bacteria in the 72 h period. The incubations were done in triplicate with annealed and unannealed films in the presence of bacteria in LB media in separate culture tubes, and the resulting bacteria from each tube were washed and dropped on three LB-agar plates to assess their viability. All values plotted are the mean ± SD, and the statistical significance is indicated using asterisks (p values < 0.0001 indicated by ****, 0.0001 to 0.001 indicated by ***, 0.001 to 0.01 indicated by **, and 0.01 to 0.05 indicated by *).

CONCLUSIONS

CZTS nanoparticles have shown potential for applications in solar cells; however, their interaction and transformation in the environment have not been thoroughly explored. This work examines the transformation of 5 and 40 nm CZTS nanoparticles and thin films produced from those nanoparticles. These transformations were considered in the greater context of assessing how the CZTS nanoparticles or thin films impacted a model environmental bacterial species under acute exposure conditions. The 5 nm diameter CZTS suspension posed significant toxicity to the bacteria model *S. oneidensis* MR-1. Dissolved ions in the suspension were partially responsible for the toxicity of the nanoparticles. Association of the nanoparticles with bacterial cells was observed using biological TEM, and significant cellular damage was obvious. In addition, CZTS dose-dependent generation of ROS was observed under abiotic conditions, suggesting a potentially important role for CZTS-induced redox chemistry. Thus, in conjunction with NP-inflicted damage to cell structures and ROS, the presence of dissolved ions also play a role in the observed toxicity of CZTS nanoparticles in suspension. Thin films were fabricated with both 5 nm and more commonly used 40 nm-diameter CZTS and were either annealed or left unannealed; none of the thin films posed significant toxicity to the bacterial cells during short-term (15 min) or longer-term (72 h) exposures. Even though ion dissolution was observed, it did not impact the colony formation ability of the bacterial cells, or at least there was significant recovery within the 72 h period in the nutrient-rich media. Thus, it can be concluded that nanoparticle size did not affect their toxicity in the thin-film form within the experimental timeframe considered here. Since thin films are more likely to be introduced into the environment than nanoparticle suspensions, this is an optimistic development from an environmental perspective. Future studies should focus on detailed mechanistic studies of any nanoscale CZTS thin-film impacts on model ecological organisms such as *Daphnia magna*, *Chironomus riparius*, and *Danio rerio* to reinforce the results obtained herein.

ASSOCIATED CONTENT

Supporting Information

The Supporting Information is available free of charge at https://pubs.acs.org/doi/10.1021/acsami.3c00374.

Chemical composition, EDS analysis, Raman spectra of CZTS nanoparticles and thin films; bacterial viability

https://doi.org/10.1021/acsami.3c00374
ACS Appl. Mater. Interfaces 2023, 15, 24978−24988

following Sn ion exposure; CZTS thin-film dissolution data in water, HEPES, and sea water; and dissolved ion concentration from CZTS nanoparticle suspensions (PDF)

AUTHOR INFORMATION

Corresponding Author

Christy L. Haynes − *Department of Chemistry, University of Minnesota, Minneapolis, Minnesota 55455, United States;* orcid.org/0000-0002-5420-5867; Email: chaynes@umn.edu

Authors

Sunipa Pramanik − *Department of Chemistry, University of Minnesota, Minneapolis, Minnesota 55455, United States;* orcid.org/0000-0001-6450-2593

Nancy Trejo − *Department of Chemical Engineering and Materials Science, University of Minnesota, Minneapolis, Minnesota 55455, United States*

Eileen Mclntire − *Department of Chemistry, University of Minnesota, Minneapolis, Minnesota 55455, United States*

Natalie V. Hudson-Smith − *Department of Chemistry, University of Minnesota, Minneapolis, Minnesota 55455, United States;* orcid.org/0000-0002-2642-0711

Beza Tuga − *Department of Chemistry, University of Minnesota, Minneapolis, Minnesota 55455, United States*

Jiayi He − *Department of Chemistry, University of Minnesota, Minneapolis, Minnesota 55455, United States*

Eray Aydil − *Department of Chemical and Biomolecular Engineering, New York University, Brooklyn, New York 11201, United States;* orcid.org/0000-0002-8377-9480

Complete contact information is available at: https://pubs.acs.org/10.1021/acsami.3c00374

Notes

The authors declare no competing financial interest.

ACKNOWLEDGMENTS

This work was supported primarily by the National Science Foundation through the University of Minnesota MRSEC under award number DMR-2011401. Part of this work was performed in the University of Minnesota College of Science and Engineering Characterization Facility, which has received capital equipment funding from the NSF through the UMN MRSEC program under award number DMR-2011401 and previous MRSEC awards. In addition, N.V.H.-S. acknowledges support through the National Science Foundation Graduate Research Fellowship Program. BST acknowledges support from the University of Minnesota Graduate School's Interdisciplinary Doctoral Fellowship. BioRender was used to create the TOC figure.

REFERENCES

(1) Meneguzzo, F.; Ciriminna, R.; Albanese, L.; Pagliaro, M. The Great Solar Boom: A Global Perspective into the Far Reaching Impact of an Unexpected Energy Revolution. *Energy Sci. Eng.* **2015**, *3*, 499.

(2) Lee, T. D.; Ebong, A. U. A Review of Thin Film Solar Cell Technologies and Challenges. *Renew. Sustain. Energy Rev.* **2017**, *70*, 1286−1297.

(3) Parida, B.; Iniyan, S.; Goic, R. A Review of Solar Photovoltaic Technologies. *Renew. Sustain. Energy Rev.* **2011**, *15*, 1625−1636.

(4) O'Regan, B.; Grätzel, M. A Low-Cost, High-Efficiency Solar Cell Based on Dye-Sensitized Colloidal TiO_2 Films. *Nature* **1991**, *353*, 737−740.

(5) Walsh, A.; Chen, S.; Wei, S.-H.; Gong, X.-G. Kesterite Thin-Film Solar Cells : Advances in Materials Modelling of Cu_2ZnSnS_4. *Adv. Energy Mater.* **2012**, *2*, 400.

(6) Oh, J.; Yuan, H. C.; Branz, H. M. An 18.2%-Efficient Black-Silicon Solar Cell Achieved through Control of Carrier Recombination in Nanostructures. *Nat. Nanotechnol.* **2012**, *7*, 743−748.

(7) Kumar, M.; Dubey, A.; Adhikari, N.; Venkatesan, S.; Qiao, Q. Strategic Review of Secondary Phases, Defects and Defect-Complexes in Kesterite CZTS-Se Solar Cells. *Energy Environ. Sci.* **2015**, *8*, 3134−3159.

(8) Mokkapati, S.; Catchpole, K. R. Nanophotonic Light Trapping in Solar Cells. *J. Appl. Phys.* **2012**, *112*, 101101.

(9) Lee, C.; Lee, G.; van der Zande, A. M.; Chen, W.; Li, Y.; Han, M.; Cui, X.; Arefe, G.; Nuckolls, C.; Heinz, T. F.; Guo, J.; Hone, J.; Kim, P. Atomically Thin p − n Junctions with van Der Waals Heterointerfaces. *Nat. Nanotechnol.* **2014**, *9*, 676−681.

(10) Mitzi, D. B.; Gunawan, O.; Todorov, T. K.; Barkhouse, A. R. D. Prospects and Performance Limitations for Cu-Zn-Sn-S-Se Photovoltaic Technology. *Philos. Trans. R. Soc., A* **2013**, *371*, 20110432.

(11) Moriya, K.; Tanaka, K.; Uchiki, H. Fabrication of Cu_2ZnSnS_4 Thin-Film Solar Cell Prepared by Pulsed Laser Deposition. *Jpn. J. Appl. Phys.* **2007**, *46*, 5780.

(12) Katagiri, H.; Jimbo, K.; Maw, W. S.; Oishi, K.; Yamazaki, M.; Araki, H.; Takeuchi, A. Development of CZTS-Based Thin Film Solar Cells. *Thin Solid Films* **2009**, *517*, 2455−2460.

(13) Shin, B.; Gunawan, O.; Zhu, Y.; Bojarczuk, N. A.; Chey, S. J.; Guha, S. Thin Film Solar Cell with 8.4% Power Conversion Efficiency Using an Earth-Abundant Cu_2ZnSnS_4 Absorber. *Prog. Photovoltaics Res. Appl.* **2013**, *21*, 72−76.

(14) Williams, B. A.; Trejo, N. D.; Wu, A.; Holgate, C. S.; Francis, L. F.; Aydil, E. S. Copper-Zinc-Tin-Sulfide Thin Films via Annealing of Ultrasonic Spray Deposited Nanocrystal Coatings. *ACS Appl. Mater. Interfaces* **2017**, *9*, 18865−18871.

(15) Zhou, H.; Hsu, W. C.; Duan, H. S.; Bob, B.; Yang, W.; Song, T. B.; Hsu, C. J.; Yang, Y. CZTS Nanocrystals: A Promising Approach for next Generation Thin Film Photovoltaics. *Energy Environ. Sci.* **2013**, *6*, 2822−2838.

(16) Woo, K.; Kim, Y.; Moon, J. A Non-Toxic, Solution-Processed, Earth Abundant Absorbing Layer for Thin-Film Solar Cells. *Energy Environ. Sci.* **2012**, *5*, 5340−5345.

(17) Wang, W.; Winkler, M. T.; Gunawan, O.; Gokmen, T.; Todorov, T. K.; Zhu, Y.; Mitzi, D. B. Device Characteristics of CZTSSe Thin-Film Solar Cells with 12.6% Efficiency. *Adv. Energy Mater* **2014**, *4*, 1301465.

(18) Guo, Q.; Hillhouse, H. W.; Agrawal, R. Synthesis of Cu_2ZnSnS_4 Nanocrystal Ink and Its Use for Solar Cells. *J. Am. Chem. Soc.* **2009**, *131*, 11672−11673.

(19) Tanaka, T.; Kawasaki, D.; Nishio, M.; Guo, Q.; Ogawa, H. Fabrication of Cu_2ZnSnS_4 Thin Films by Co-Evaporation. *Phys. Status Solidi C* **2006**, *3*, 2844−2847.

(20) Jeon, M.; Tanaka, Y.; Shimizu, T.; Shingubara, S. Formation and Characterization of Single-Step Electrodeposited Cu_2ZnSnS_4 Thin Films: Effect of Complexing Agent Volume. *Energy Procedia* **2011**, *10*, 255−260.

(21) Steinhagen, C.; Panthani, M. G.; Akhavan, V.; Goodfellow, B.; Koo, B.; Korgel, B. A. Synthesis of Cu_2ZnSnS_4 Nanocrystals for Use in Low-Cost Photovoltaics. *J. Am. Chem. Soc.* **2009**, *131*, 12554−12555.

(22) Todorov, T. K.; Reuter, K. B.; Mitzi, D. B. High-Efficiency Solar Cell with Earth-Abundant Liquid-Processed Absorber. *Adv. Mater.* **2010**, *22*, E156−E159.

(23) Kumar, R. S.; Maddirevula, S.; Easwaran, M.; Dananjaya, S. H. S.; Kim, M. D. Antibacterial Activity of Novel Cu_2ZnSnS_4 Nanoparticles against Pathogenic Strains. *RSC Adv* **2015**, *5*, 106400−106405.

(24) Feng, Z. V.; Gunsolus, I. L.; Qiu, T. A.; Hurley, K. R.; Nyberg, L. H.; Frew, H.; Johnson, K. P.; Vartanian, A. M.; Jacob, L. M.; Lohse,

S. E.; Torelli, M. D.; Hamers, R. J.; Murphy, C. J.; Haynes, C. L. Impacts of Gold Nanoparticle Charge and Ligand Type on Surface Binding and Toxicity to Gram-Negative and Gram-Positive Bacteria. *Chem. Sci.* **2015**, *6*, 5186−5196.
(25) Pramanik, S.; Hill, S. K. E.; Zhi, B.; Hudson-Smith, N. V.; Wu, J. J.; White, J. N.; McIntire, E. A.; Kondeti, V. S. S. K.; Lee, A. L.; Bruggeman, P. J.; Kortshagen, U. R.; Haynes, C. L. Comparative Toxicity Assessment of Novel Si Quantum Dots and Their Traditional Cd-Based Counterparts Using Bacteria Models *Shewanella oneidensis* and *Bacillus subtilis*. *Environ. Sci. Nano* **2018**, *5*, 1890−1901.
(26) Chernomordik, B. D.; Béland, A. E.; Trejo, N. D.; Gunawan, A. A.; Deng, D. D.; Mkhoyan, K. A.; Aydil, E. S. Rapid Facile Synthesis of Cu_2ZnSnS_4 Nanocrystals. *J. Mater. Chem. A* **2014**, *2*, 10389−10395.
(27) Chernomordik, B. D.; Béland, A. E.; Deng, D. D.; Francis, L. F.; Aydil, E. S. Microstructure Evolution and Crystal Growth in Cu_2ZnSnS_4 Thin Films Formed by Annealing Colloidal Nanocrystal Coatings. *Chem. Mater.* **2014**, *26*, 3191−3201.
(28) Tosun, B. S.; Chernomordik, B. D.; Gunawan, A. A.; Williams, B.; Andre Mkhoyan, K.; Francis, L. F.; Aydil, E. S. Cu_2ZnSnS_4 Nanocrystal Dispersions in Polar Liquids. *Chem. Commun.* **2013**, *49*, 3549−3551.
(29) Todorov, T. K.; Tang, J.; Bag, S.; Gunawan, O.; Gokmen, T.; Zhu, Y.; Mitzi, D. B. Beyond 11% Efficiency: Characteristics of State-of-the-Art $Cu_2ZnSn(S,Se)_4$ Solar Cells. *Adv. Energy Mater.* **2013**, *3*, 34−38.
(30) Khare, A.; Wills, A. W.; Ammerman, L. M.; Norris, D. J.; Aydil, E. S. Size Control and Quantum Confinement in Cu_2ZnSnS_4 Nanocrystals. *Chem. Commun.* **2011**, *47*, 11721−11723.
(31) Zhi, B.; Mishra, S.; Hudson-Smith, N. V.; Kortshagen, U. R.; Haynes, C. L. Toxicity Evaluation of Boron- And Phosphorus-Doped Silicon Nanocrystals toward *Shewanella oneidensis* MR-1. *ACS Appl. Nano Mater.* **2018**, *1*, 4884−4893.
(32) Zhang, H.; Pokhrel, S.; Ji, Z.; Meng, H.; Wang, X.; Lin, S.; Chang, C. H.; Li, L.; Li, R.; Sun, B.; Wang, M.; Liao, Y. P.; Liu, R.; Xia, T.; Mädler, L.; Nel, A. E. PdO Doping Tunes Band-Gap Energy Levels as Well as Oxidative Stress Responses to a Co_3O_4 p -Type Semiconductor in Cells and the Lung. *J. Am. Chem. Soc.* **2014**, *136*, 6406−6420.
(33) Jiang, M.; Y, X. Cu_2ZnSnS_4 Thin Film Solar Cells: Present Status and Future Prospects. *Solar Cells—Research and Application Perspectives*; InTech, 2013.
(34) Camara, S. M.; Wang, L.; Zhang, X. Easy Hydrothermal Preparation of Cu_2ZnSnS_4 (CZTS) Nanoparticles for Solar Cell Application. *Nanotechnology* **2013**, *24*, 495401.
(35) Kittler, S.; Greulich, C.; Diendorf, J.; Köller, M.; Epple, M. Toxicity of Silver Nanoparticles Increases during Storage Because of Slow Dissolution under Release of Silver Ions. *Chem. Mater.* **2010**, *22*, 4548−4554.
(36) Hang, M. N.; Gunsolus, I. L.; Wayland, H.; Melby, E. S.; Mensch, A. C.; Hurley, K. R.; Pedersen, J. A.; Haynes, C. L.; Hamers, R. J. Impact of Nanoscale Lithium Nickel Manganese Cobalt Oxide (NMC) on the Bacterium *Shewanella oneidensis* MR-1. *Chem. Mater.* **2016**, *28*, 1092−1100.
(37) Qiu, T. A.; Guidolin, V.; Hoang, K. N. L.; Pho, T.; Carra', A.; Villalta, P. W.; He, J.; Yao, X.; Hamers, R. J.; Balbo, S.; Feng, Z. V.; Haynes, C. L. Nanoscale Battery Cathode Materials Induce DNA Damage in Bacteria. *Chem. Sci.* **2020**, *11*, 11244−11258.
(38) Abdullah, A. A. M.; King, P. E. Synergistic Effects of Zinc and Copper Ions in a Freshwater Isopod *Asellus aquaticus* (L.). *J.Basrah Res.* **2004**, *30*. DOI: 10.13140/RG.2.2.13712.20488.
(39) Şengör, S. S.; Barua, S.; Gikas, P.; Ginn, T. R.; Peyton, B.; Sani, R. K.; Spycher, N. F. Influence of Heavy Metals on Microbial Growth Kinetics Including Lag Time: Mathematical Modeling and Experimental Verification. *Environ. Toxicol. Chem.* **2009**, *28*, 2020−2029.
(40) Ochoa-Herrera, V.; León, G.; Banihani, Q.; Field, J. A.; Sierra-Alvarez, R. Toxicity of Copper(II) Ions to Microorganisms in Biological Wastewater Treatment Systems. *Sci. Total Environ.* **2011**, *412*−*413*, 380−385.
(41) Groisman, E. A.; Hollands, K.; Kriner, M. A.; Lee, E. J.; Park, S. Y.; Pontes, M. H. Bacterial Mg^{2+} Homeostasis, Transport, and Virulence. *Annu. Rev. Genet.* **2013**, *47*, 625−646.
(42) Klein, N. D.; Hurley, K. R.; Feng, Z. V.; Haynes, C. L. Dark Field Transmission Electron Microscopy as a Tool for Identifying Inorganic Nanoparticles in Biological Matrices. *Anal. Chem.* **2015**, *87*, 4356−4362.
(43) Nosaka, Y.; Nosaka, A. Y. Generation and Detection of Reactive Oxygen Species in Photocatalysis. *Chem. Rev.* **2017**, *117*, 11302−11336.
(44) George, S.; Pokhrel, S.; Ji, Z.; Henderson, B. L.; Xia, T.; Li, L.; Zink, J. I.; Nel, A. E.; Mädler, L. Role of Fe Doping in Tuning the Band Gap of TiO_2 for the Photo-Oxidation-Induced Cytotoxicity Paradigm. *J. Am. Chem. Soc.* **2011**, *133*, 11270−11278.
(45) Escamilla-Rivera, V.; Uribe-Ramirez, M.; Gonzalez-Pozos, S.; Velumani, S.; Arreola-Mendoza, L.; De Vizcaya-Ruiz, A. Cytotoxicity of Semiconductor Nanoparticles in A549 Cells Is Attributable to Their Intrinsic Oxidant Activity. *J. Nanoparticle Res.* **2016**, *18*, 85.
(46) Yin, J.; Gao, H. Stress Responses of Shewanella. *Int J Microbiol.* **2011**, *2011*, 863623.